ElasticDiffusion: Training-free Arbitrary Size Image Generation through Global-Local Content Separation

Moayed Haji-Ali   Guha Balakrishnan   Vicente Ordonez

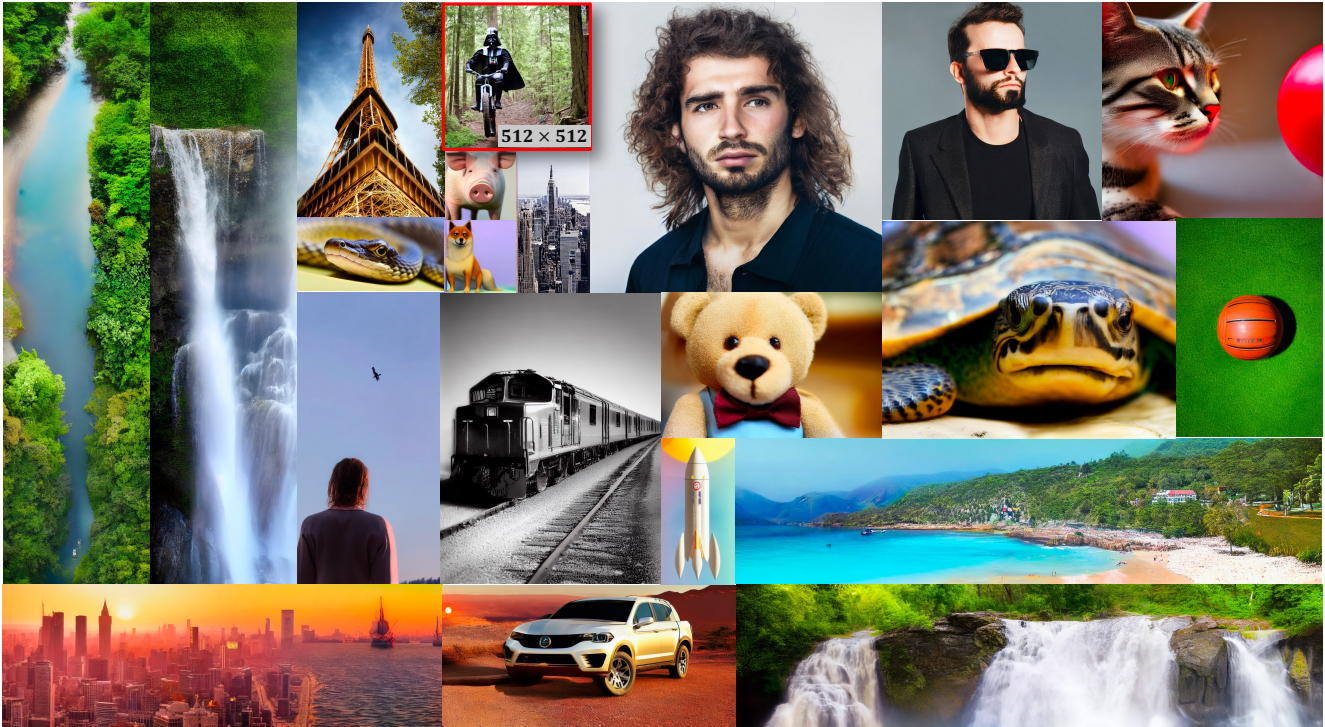Rice University

{mh155, guha, vicenteor}@rice.edu

Figure 1. **ElasticDiffusion** generates high quality images at arbitrary sizes using a pretrained diffusion model trained on a single image size, with equivalent memory footprint and no further training. These results are based on Stable Diffusion$_{1.4}$, which was trained to generate 512×512 images. The examples shown in this collage are presented without any image cropping, stretching, or post-processing.

Abstract

Diffusion models have revolutionized image generation in recent years, yet they are still limited to a few sizes and aspect ratios. We propose ElasticDiffusion, a novel training-free decoding method that enables pretrained text-to-image diffusion models to generate images with various sizes. ElasticDiffusion attempts to decouple the generation trajectory of a pretrained model into local and global signals. The local signal controls low-level pixel information and can be estimated on local patches, while the global signal is used to maintain overall structural consistency and is estimated with a reference image. We test our method on CelebA-HQ (faces) and LAION-COCO (objects/indoor/outdoor scenes). Our experiments and qualita-
tive results show superior image coherence quality across aspect ratios compared to MultiDiffusion and the standard decoding strategy of Stable Diffusion. Project Webpage: https://elasticdiffusion.github.io/

1. Introduction

Diffusion models are a powerful family of algorithms that achieve remarkable quality and obtain the current state-of-the-art performance on various image synthesis tasks. As is the case with most deep neural networks, diffusion models are typically trained on one or a few image resolutions. For instance, Stable Diffusion (SD) [43], one of the most widely adopted diffusion models, is trained on a square images of size 512 x 512, yet fails to maintain its performance at dif-

1

ferent aspect ratios during inference time. In practice, many applications require a wide aspect ratio or portrait mode, such as digital billboards, wearable devices, automotive displays, and any application relying on a computer screen.

Recent studies address the issue of variable image size in different ways. SDXL [39] and Any-Size-Diffusion [68] explicitly finetune models on images with a range of aspect ratios, which requires extensive computation, a quadratic memory footprint, and larger training data. In addition, this strategy requires a set of resolutions to be specified upfront during training time, while the models still struggle to generalize to new resolutions during inference, often resulting in artifacts. Recent works also show remarkable results in generating panoramic images using pretrained diffusion models by overlapping generated patches into a larger image [3, 69]. These methods work well for landscape images with repetitive patterns. However, their lack of global guidance limits their abilities to generate images of single objects or faces where global structure is important. Recent work [26, 56, 57] aimed at extending pre-trained diffusion models capabilities to others domains, often in a training-free way [4, 7, 14, 31, 33, 38, 52, 60, 67]. Few concurrent work [9, 10, 12, 34, 66] focus on adapting them to higher resolutions, yet they are constrained to square images.

In this work, we propose ElasticDiffusion, a novel decoding strategy that takes a pretrained diffusion model and generate images at arbitrary sizes during inference using a constant memory footprint. To achieve this, we revisit the guidance mechanism of conditional diffusion models to decouple global and local content generation. Global content controls the high-level aspects of the image, whereas local content adds finer, more granular details. This separation facilitates generating the local content in patches for images of varying sizes, all while being guided with global content that we derive from a reference image at the diffusion model pretraining resolution. This enables the synthesis of images at diverse resolutions and aspect ratios while adhering the diffusion forward calls to the model's initial training size. To aid in this task, we introduce several techniques including an *efficient* patch fusion method for smooth boundaries, a novel guidance strategy to reduce image artifacts, and a global content resampling technique that amplifies the resolution of diffusion models up to 4X the training size.

Figure 1 shows a diverse array of images generated with ElasticDiffusion. Several of theses images include a single object or were generated with extreme aspect ratios, showcasing our method's ability to produce coherent images under various sizes. Quantitatively, ElasticDiffusion outperforms baselines across most aspect ratios. More importantly, despite relying on Stable Diffusion$_{1.4}$, ElasticDiffusion obtains comparable FID (228.87 vs 230.21) and CLIP scores (26.07 vs 28.06) as SDXL when generating images at 1024×1024, which is the native resolution of SDXL.

2. Related Work

Diffusion Models have been widely adopted for their high-quality outputs in generative tasks [8, 11, 16, 21, 23, 39, 41, 43, 47, 61, 64]. These models involve iterative decoding with many steps leading to high compute and memory requirements. Recent work addressed these issues by devising faster sampling strategies [29, 54], hierarchical models [20, 41, 47], progressive training at increasing resolutions [36, 39, 43], and two-stage models [39, 43, 46, 59]. Stable Diffusion (SD) [43] trains a variational auto-encoder to compress images into a low-dimensional 64×64 latent space and trains a diffusion model on this latent space. To train for higher resolutions, models are initially trained at a 256×256 resolution, before fine-tuning them at 512×512 and 1024×1024 in the case of SDXL [39]. SD is one of the few large-scale diffusion models that released trained parameters, making it the building block for many subsequent work [5, 17, 44, 48, 58, 59]. However, these models, including SD, are confined to specific resolutions and do not generalize well to aspect ratios unseen during training. Interestingly, despite being presented with a 256×256 resolution during their early training stages, both SD and SDXL fail to generate realistic images at this resolution after being fine-tuned for larger outputs. ElasticDiffusion enables high quality generation at unseen resolutions including re-enabling consistent high quality outputs for SD at 256×256.

Mixture of diffusers [69] and *MultiDiffusion* [3] generate panoramic images using a pre-trained diffusion model by generating overlapping crops and combining the generation signal of the overalpping regions. Blending multiple generation signals spatially has been of interest in many previous work [1, 69]. *SDXL* [39] and *Any-Size-Diffusion* [68] finetune a pre-trained SD on a fixed set of resolutions. A concurrent work [15] uses dilated convolution kernels to reduce SD artifacts when generating non-square images. ElasticDiffusion extends a pre-trained SD to generate images of various sizes at a constant memory requirement and without additional training, all while ensuring global coherence.

Guided diffusion models devise strategies to condition image generation based on text and other modalities [2, 2, 6, 19, 25, 28, 35, 43, 63, 65]. Classifier guidance [35] uses a pre-trained classifier on noisy images to guide the generation process. Classifier-free guidance [19] eliminates the need for a pretrained classifier but requires training a conditional diffusion model, limiting its applications. Universal Guidance [2] applies a pre-trained classifier on the noise-free images produced by DDIM [54], bypassing training on noisy images. StableSR [59] uses LoRA [22] to condition the generation on low-resolution inputs to achieve superb image super-resolution. Inspired by this, we propose Reduce-Resolution Guidance (Sec. 4) to constrain the generation of high-res images using a lower resolution version, substantially reduceing artifacts without extra training.

3. Background: Diffusion Models

A conditional diffusion model $\epsilon_\theta \colon \mathcal{X} \times \mathcal{C} \to \mathcal{X}$ predicts a less noisy version of the input image $x \in \mathbb{R}^{H \times W \times 3}$, conditioned on variable $c \in \mathbb{R}^D$ (*e.g.* a text embedding). Starting with $x_T \sim \mathcal{N}(0, \mathbf{I})$, the reverse diffusion process progressively denoise x_T over T steps to generate a realistic image x_0 that conforms to the input condition c through:

$$x_{t-1} = \epsilon_\theta(x_t, c) \qquad \text{for } t = T, T-1, \dots, 1,$$

where ϵ_θ is the denoising network. Standard diffusion models operate in the pixel space, but others like Latent Diffusion Models [43] instead operate on a latent image encoding space to reduce memory footprints. A U-Net architecture is commonly used to implement the denoising network and is typically trained on images at a fixed resolution $H \times W$ [8, 43, 47]. The convolutional architecture of a U-Net allows for inputs and outputs of *arbitrary spatial dimensions*. In order to generate an image of a different size $\bar{H} \times \bar{W}$ at inference time, one can sample an initial noise variable $\bar{x}_T \in \mathbb{R}^{\bar{H} \times \bar{W} \times 3}$ and follow the same diffusion process. However, we find that this works poorly in practice, resulting in a significant degradation in output quality.

Denoising Diffusion Implicit Models (DDIMs) introduce a faster non-Markovian sampling strategy, bypassing denoising steps. The reverse diffusion step in DDIM is:

$$x_{t-1} = \sqrt{\bar{\alpha}_{t-1}} \underbrace{\left(\frac{x_t - \sqrt{1 - \bar{\alpha}_t} \epsilon_\theta^{(t)}(x_t)}{\sqrt{\bar{\alpha}_t}} \right)}_{\text{predicted } \hat{x}_0^t} + \underbrace{\sqrt{1 - \bar{\alpha}_{t-1}}}_{\substack{\text{direction} \\ \text{pointing} \\ \text{to } x_t}}, \quad (1)$$

where $\bar{\alpha}_t = \prod_{i=1}^t 1 - \beta_i$ is a cumulative product of the noise levels using a predetermined variance schedule β. $\hat{x}_0^t$ is a noise-free estimation of x_t obtained by subtracting the predicted noise scaled for step t. We assume a deterministic sampling process in the DDIM formula [54] for simplicity.

Classifier-Free Guidance updates the reverse diffusion process to condition it on a given condition c as:

$$\hat{\epsilon}_\theta^{(t)}(x_t) = \underbrace{\epsilon_\theta^{(t)}(x_t)}_{\substack{\text{unconditional} \\ \text{score}}} + (1+w) \cdot \underbrace{(\epsilon_\theta^{(t)}(x_t, c) - \epsilon_\theta^{(t)}(x_t))}_{\Delta_{\mathcal{C}}(x, c)\colon \text{class direction score}}. \quad (2)$$

$\epsilon_\theta(x, c)$ is a pretrained conditional diffusion model, and w is a scaling factor. The difference between the conditional $\epsilon_\theta(x, c)$ and unconditional $\epsilon_\theta(x)$ scores, denoted as *class direction score*, gives the guidance direction towards c.

4. ElasticDiffusion

The aim of this work is to develop a method capable of synthesizing images at arbitrary size $\bar{H} \times \bar{W}$, and conforming
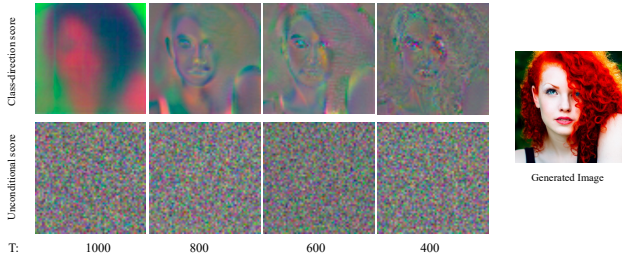

Figure 2. **PCA of diffusion scores:** class-direction score (top) dictates global content by clustering on semantic parts, while the unconditional score (bottom) lacks pixel correlations.

to a global condition c using a pre-trained diffusion model that is limited at inference to its training resolution $H \times W$. To achieve this, we observe a main insight with respect to the diffusion scores in Eq. (2) that we visualize in Fig. 2. The class direction score (Δ_c) primarily dictates the image's overall composition by showing clustering along semantic regions (*e.g.* hair) and edges. Thus, upscaling this score maintains global content in higher resolutions. In contrast, the unconditional score lacks inter-pixel correlation, suggesting a localized influence in enhancing detail at the pixel level. Thus, computing it requires a pixel-level precision. We study the global and local behaviour of these scores in Supp. Sec. 8.2. Our intuition behind this observation is that latent pixels, specifically in early diffusion steps where noise is high, display weak and short-range correlations. This leads the unconditional score to focus on local patterns due to these limited pixel interactions. Meanwhile, as Δ_c represents a latent direction towards a specified global condition, it exerts a global influence by guiding clusters of pixels with similar directions towards semantic regions, overriding their initial noisy state. Leveraging this insight, we propose a method to decouple the generation of local and global content during the diffusion process. Specifically, we compute the unconditional score on local patches of size $H \times W$ while simultaneously resizing a class direction score, originally derived for a reference latent of the dimensions $H \times W$ as well. This dual strategy facilitates the generation of images at varied sizes using a pretrained diffusion model at its native resolution, all while maintaining the same memory requirement and without further training. We first present our approach for computing the unconditional score (Sec. 4.1). We then detail our method to estimate (Sec. 4.2) and upscale the resolution (Sec. 4.3) of the class direction score. Finally, we combine the two estimated scores with a novel guidance strategy to generate images at arbitrary sizes (Sec. 4.4). The generation process of ElasticDiffusion is illustrated in Fig. 3.

4.1. Estimating the Unconditional Score

Building upon previous work [3, 59, 69], we estimate the unconditional score for a large latent signal $\bar{x}_t \in \mathbb{R}^{\bar{H} \times \bar{W} \times 3}$ by concatenating scores derived from local patches. Specif-
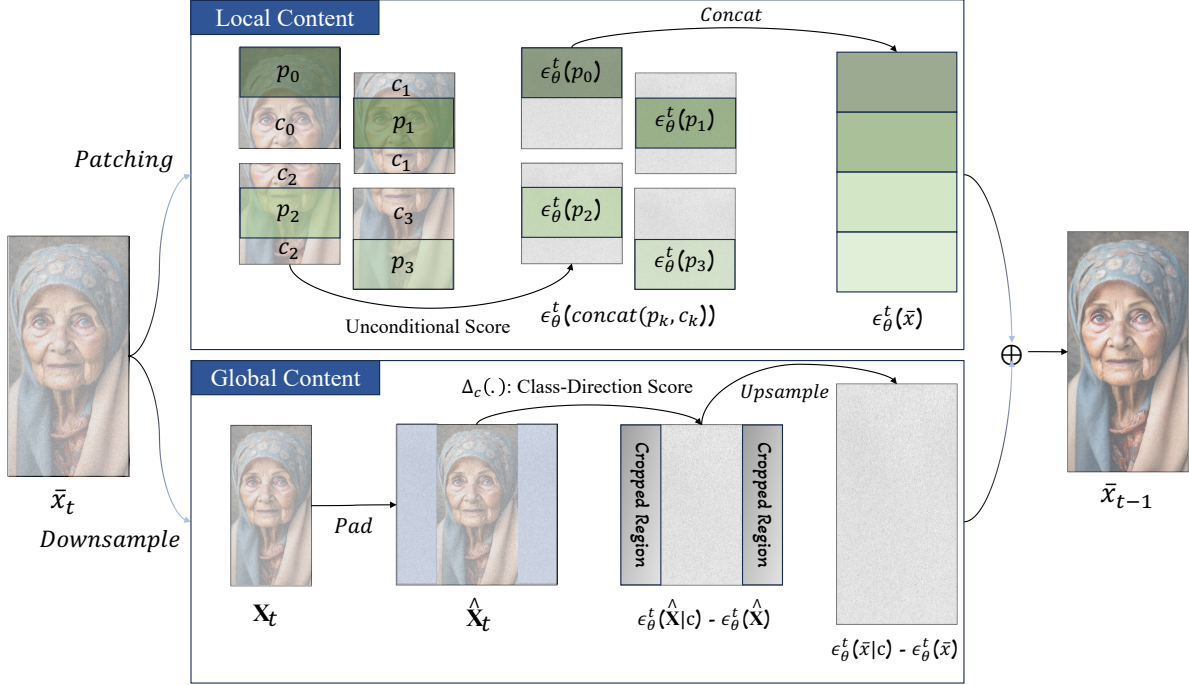
Figure 3. **Illustration of ElasticDiffusion:** We generate images at various sizes by generating local and global content separately. For local content, we partition the latent $\bar{x}_t$ into *non-overlapping* patches p_k, each concatenated with context c_k to estimate their unconditional score. For global content, we downsample $\bar{x}_t$ to $\mathbf{x}_t$, pad to a square size ($\hat{\mathbf{x}}_t$), compute class-direction score (Δ_c), and upscale to match $\bar{x}_t$.

ically, we divide image $\bar{x}_t$ to K patches $P_k \in \mathbb{R}^{H \times W \times 3}$ and compute the score as $\epsilon_\theta(\bar{x}_t) = \{\epsilon_\theta(P_k); \ \forall_{k \leq K}\}$. A common challenge encountered with this implementation is discontinuities at boundaries, as illustrated in Fig. 4 (A). To address this, earlier research calculated the diffusion model score on explicitly overlapping patches and averaged their scores in the intersecting regions [3, 59, 69]. While this strategy mitigates discontinuities, it requires large overlap between patches, thereby substantially increasing inference time and blurring details. To speed up the process, we introduce a more effective method that enhances boundary transitions in local patches by incorporating contextual information from adjacent patches, thus negating the need for signal averaging in overlapping areas. Specifically, we select patches smaller than the full size $p_k \in \mathbb{R}^{h \times w \times 3}$ with $h < H$ and $w < W$, and concatenate them with context pixels from adjacent patches, denoted as $c_k \in \mathbb{R}^{(H-h) \times (W-w) \times 3}$, to compute the diffusion model unconditional score $\mathbf{S}_u$ as:

$$\tilde{\epsilon}_\theta(x_t) = \{\, \epsilon_\theta(p_k \mid c_k) \mid \bar{x}_t = \{p_k; \ \forall_{k \leq K}\}\}, \qquad (3)$$

where p_i is a local patch and c_i are the context pixels surrounding it. This substantially increases the efficiency of the process. For instance, to generate an image of size 1024×1024, previous methods [3, 59, 69] used 87.5% overlap between adjacent patches, necessitating 81 forward diffusion calls per decoding step. In comparison, ElasticDiffusion achieves comparable results with only 9 forward calls,

as demonstrated in Fig. 4 (D). Employing the same number of calls, previous techniques result in obvious boundary discontinuities, as depicted in Fig. 4 (B).

4.2. Estimating the Class Direction Score

A simple approach to estimate a class direction score of an intermediate latent signal $\bar{x}_t \in \mathbb{R}^{\bar{H} \times \bar{W} \times 3}$ is to upsample the score from a reference latent $x_t \in \mathbb{R}^{N \times M \times 3}$ to $\bar{H} \times \bar{W}$. This is possible due to our observation that the class direction score represents a latent direction that can be shared between nearby pixels. We validate this observation empirically in Supp. Sec. 8.2. We choose $N < H$ and $M < W$ such that $N \times M$ is as close as possible to $H \times W$ and $\frac{\bar{H}}{\bar{W}} = \frac{N}{M}$. This is important to maintain the aspect ratio and prevent stretching the global content. Formally, we compute the class direction score $\mathbf{S}_d$ as:

$$\begin{aligned} \mathbf{x}_t &\leftarrow \text{Downsample}(\bar{x}_t, N \times M), \\ \Delta_{\mathcal{C}}(\bar{x}_t, c) &= \text{Upsample}(\Delta_{\mathcal{C}}(\mathbf{x}_t, c), \bar{H} \times \bar{W}), \end{aligned} \qquad (4)$$

where $\Delta_{\mathcal{C}}(.)$ is the class direction score from Eq. (2), Downsample and Upsample are downsampling and upsampling operations. We use a nearest-neighbors approach to prevent altering the statistics of the latent signal. In order to maintain the input to the diffusion models at the size $H \times W$, we dynamically pad the downsampled latent $\mathbf{x}_t$ using a random background with a constant color.
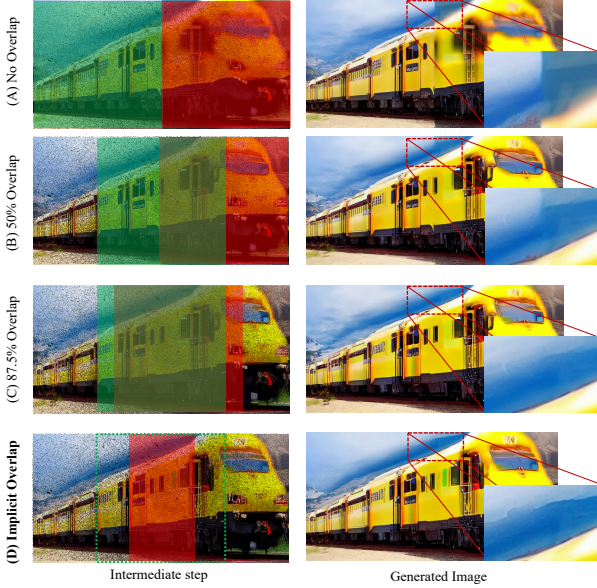
4

Figure 4. Comparing strategies for calculating diffusion model score on a local patch. No overlap between adjacent patches (A) leads to discontinuities at the boundaries. Strategies (B) and (C), explicitly overlap nearby patches, necessitating substantial overlap to be effective. Our implicit overlapping method (D) achieves superior results with computational demand similar to (B).

This encourages the model to concentrate content generation within the center area. We then crop the extended parts from the predicted noise to the target image resolution $N \times M$. Formally we modify the forward call for the reverse diffusion step as:

$$\hat{\mathbf{x}}_t \leftarrow \text{Pad}\left(\mathbf{x}_t, \mathcal{A}_t\sqrt{\bar{\alpha}_t} + \sqrt{1 - \bar{\alpha}_t} \cdot \mathcal{Z}_t\right),$$
$$\epsilon_\theta\left(\mathbf{x}_t, c\right) = \text{Crop}\left(\epsilon_\theta\left(\hat{\mathbf{x}}_t, c\right), N \times M\right), \quad (5)$$

where $\mathcal{Z}_t \sim \mathcal{N}(0, I)$ represents the injected Gaussian noise at each step, and $\mathcal{A}_t$ represents a background image of size $(H-N) \times (W-M)$ with a constant color value $\mathcal{Y}$ randomly sampled from a uniform distribution. This simple padding operation guarantees that the input to the diffusion model is kept at $H \times W$, while encouraging the diffusion model to keep the generated content within the cropped $N \times M$ center that we are interested in.

4.3. Refined Class Direction Score

Sharing the class direction score among nearby pixels can result in over-smoothed images. To mitigate this, we propose an iterative resampling technique that increases the resolution of the estimated class direction score by extrapolating missing image components from their surrounding context, following [32]. Our technique involves a gradual enhancement of the class direction score's resolution by estimating and integrating it for newly sampled pixels. Specifically, in each iteration, we replace $n\%$ of the pixels
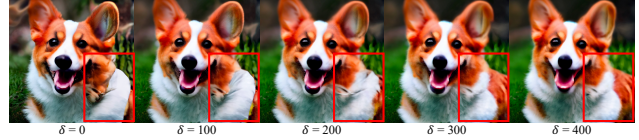

Figure 5. **The Effect of Reduced-Resolution Guidance (RRG).** Higher RRG weights effectively eliminates emerging artifacts albeit at the cost of slightly blurrier outputs. $\delta = 200$ strikes a good balance. Improvements are more noticeable when zooming in.

Figure 6. **Effect of Resampling.** Applying more resampling steps noticeably enhances detail in the generated images.

in $\mathbf{x}_t$ with newly sampled ones from x_t to get an updated version $\tilde{\mathbf{x}}_t$. Following each update, the direction score is recalculated and blended with the previously calculated score. Formally, we consider $\mathbf{S}_d^0 = \mathbf{S}_d$ and define the iterative resampling as:

$$\mathbf{S}_d^{r+1} = \mathbf{S}_d^r \odot m + \tilde{\mathbf{S}}_d \odot (1 - m), \quad (6)$$

where $m \in \{0, 1\}^{\bar{H} \times \bar{W}}$ is a mask with a value of 1 at the positions of the newly sampled pixels and 0 elsewhere. $\tilde{\mathbf{S}}_d$ represents the recalculated class direction score on $\tilde{\mathbf{x}}_t$ as per Eq. (4). This method estimates the class direction score of $n\%$ new pixels while retaining the information of the previously estimated score, thereby increasing the score's overall resolution. In our experiments, we set n to 20% and repeat the process R times, depending on the target generation resolution. Fig. 6 demonstrates the effectiveness of our method in enhancing the details of the generated images.

4.4. Reduced-Resolution Guidance (RRG)

We effectively estimate the unconditional score signal and concurrently steer the image generation using the class direction score. However, inaccuracies in unconditional score estimation or fluctuations in local content, especially from distant patches, can lead to artifacts. To enhance image coherence and diminish artifacts, we consider a downsampled version of the latent at each decoding step as a reference and aim to align the decoded latent with it through our reduced-resolution latent update strategy. Specifically, we utilize the noise-free sample $\hat{x}_0^t$ of the latent x_t from Eq. (1) and generate a corresponding noise-free sample $\hat{\mathbf{x}}_0^t$ from its downsampled counterpart $\mathbf{x}^t$ in Eq. (4) as:

$$\hat{\mathbf{x}}_0^t = \frac{1}{\sqrt{\bar{\alpha}_t}}(\mathbf{x}_t - \sqrt{1 - \bar{\alpha}_t} \cdot (\epsilon_\theta(\mathbf{x}_t) + (1 + w) \cdot \Delta_\mathcal{C}(\mathbf{x}_t, c))),$$

Here, both $\hat{x}_0^t$ and $\hat{\mathbf{x}}_0^t$ corresponds to the same latent update at different resolutions. Due to its smaller dimension, $\hat{\mathbf{x}}_0^t$ has a broader context when computing the unconditional

Figure 7. **Qualitative comparison at various resolutions on CelebAHQ faces.** *ElasticDiffusion* consistently generates coherent images at all resolutions. *StableDiffusion*, and *MultiDiffusion* produce repeating body parts at higher resolutions, while *StableDiffusion-XL* fails to maintain its quality at lower resolutions, resulting in noisy outputs at 256×256. We exclude *MultiDiffusion* results at 256×256 as it is not designed to produce images at lower resolutions.

signal. To guide x_t with its downsampled reference, we refine the latent x_t with the direction that minimizes $L2$ difference between $\hat{\mathbf{x}}_0^t$ and $\hat{x}_0^t$. Formally,

$$\bar{x}_{t-1} \leftarrow \bar{x}_{t-1} - \delta_t \nabla_{x_t} ||\text{Upsample}(\hat{\mathbf{x}}_0^t, \bar{H} \times \bar{W}) - \hat{x}_0^t||, \quad (7)$$

where δ_t represent the weight of the guidance. Since the overall image structure is determined in the early diffusion steps, we start with $\delta_t = 400$ and follow a cosine scheduler to decrease this weight for later diffusion steps. This scheduling strategy mitigates potential quality degradation from matching the generated image with a lower-resolution version while allowing the model to fill-in higher-resolution details in the later decoding stages. Fig. 5 illustrates how RRG eliminates emerging artifacts.

5. Experiments

ElasticDiffusion supports generating images across different resolutions and aspect ratios. Our experiments focus on: (1) square images at multiple resolutions, and (2) images with varied aspect ratios and resolutions.

Datasets. We evaluate the generation of square images on the Multi-Modal CelebAHQ dataset [62], which includes high-resolution square face images accompanied with text descriptions. We evaluate different aspect ratio generation using the LAION-COCO dataset [50], derived from the web-crawled LAION-5B dataset [49], which includes a variety of image aspect ratios and contains landscapes, people,

objects, and everyday scenes, each paired with a synthetic caption generated using BLIP [30]. We consider four common aspect ratios: 9:16, 16:9, 3:4 and 4:3.

Evaluation Metrics. Following prior text-to-image synthesis works [3, 36, 39, 42, 47], we use automatic evaluation metrics *Frechet Inception Distance (FID)* and *CLIP-score*. *FID* [18] measures both the realism and diversity of the generated images by calculating the difference between features of the real and generated images computed using Inception-V3 [55] pretrained on ImageNet [45]. *CLIP-score* uses a pretrained text-image CLIP model [40] to measure alignment between the generated images and input prompts. We use 10,000 images to compute these scores.

Baselines. We compare our approach against prior diffusion model generation methods, specifically focusing on *Stable Diffusion (SD)* and *MultiDiffusion (MD)*. *SD* follows the standard reverse diffusion process on an image latent space. *MD* uses a pretrained *SD* for panoramic image generation, by creating smaller, overlapping patches and averaging the Diffusion Model scores in intersecting areas. For baseline comparisons, we fix the pre-trained diffusion model to $SD_{1.4}$, which is trained to generate images at a resolution of 512×512. Additionally, we compare our method with *SDXL*, an enhanced SD model that is three times larger than the standard one. SDXL is trained at a higher resolution of $1024p$, and fine-tuned on a specific set of aspect ratios with pixel sums close to 1024^2. We exclude
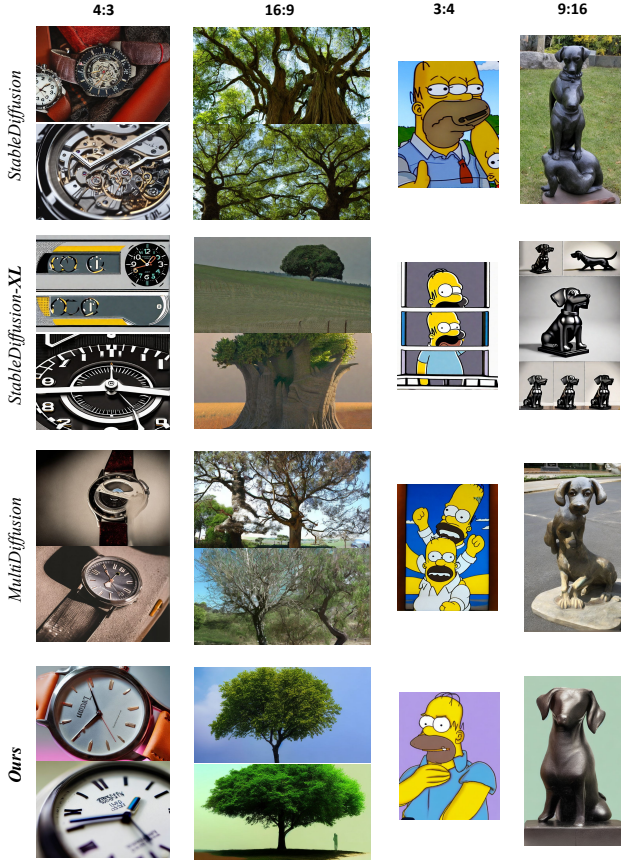
Figure 8. **Qualitative comparison on various aspect ratios.** *ElasticDiffusion* effectively handles a variety of aspect ratios. In comparison, *SD* and *MultiDiffusion* generate unrealistic images, while *SDXL* outputs exhibit a decline in the perceptual quality.

the latent refinement module in *SDXL* and focus our analysis on the base model. Throughout our experiments, we employ a DDIM sampling strategy with 50 steps and use 7.0 for the classifier-free guidance scaling factor. We also ensure consistency in seeds and captions for all baselines.

5.1. Qualitative Results

We show square image generation samples in Fig. 7 generated from the CelebAHQ dataset at various resolutions. Both *MultiDiffusion* and *Stable Diffusion* have a tendency to replicate textures and body parts at higher resolutions, resulting in images that lack coherence. At resolutions lower than its training resolution 512×512, *StableDiffusion* aligns poorly with the provided captions and produces unappealing images. *SDXL*, trained for 1024×1024 resolution, has a similar trend of reduced perceptual quality at lower sizes, eventually producing complete noise at a resolution of 256×256. In contrast, ElasticDiffusion maintains image coherence across all tested resolutions, and yields results comparable to *SDXL* at 1024×1024, despite using a less powerful base model and lower memory. We excluded

Table 1. Quantitative comparison of on CelebA-HQ and LAION-COCO at different resolution. We indicate the best performances in **bold**, and underline the second best ones. $\#Calls$ represent the number of diffusion model calls required at each decoding steps.

Res.	Method	CelebA-HQ		LAION-COCO		#Calls	Mem.
		FID ↓	CLIP ↑	FID ↓	CLIP ↑		
256 × 256	SD$_{1.4}$	<u>258.43</u>	<u>20.14</u>	<u>54.06</u>	<u>21.43</u>	2	7.2GB
	SDXL	368.06	14.40	175.87	14.60	2	18.5GB
	Ours$_{1.4}$	**235.23**	**23.88**	**23.77**	**26.30**	2	8.6GB
512 × 512	SD$_{1.4}$	233.40	24.00	20.50	27.33	2	8.6GB
	SDXL	240.20	21.57	42.58	25.34	2	21.6GB
768 × 768	SD$_{1.4}$	238.87	23.45	29.89	27.01	2	11.1GB
	MD$_{1.4}$	240.56	22.82	29.98	<u>27.31</u>	50	8.6GB
	SDXL	**225.48**	<u>24.23</u>	**23.31**	**27.88**	2	24.5GB
	Ours$_{1.4}$	<u>225.86</u>	**26.66**	<u>25.78</u>	25.93	17	8.6GB
1024 × 1024	SD$_{1.4}$	266.01	21.90	47.01	25.70	1	14.7GB
	MD$_{1.4}$	264.57	21.55	37.70	<u>26.96</u>	162	8.6GB
	SDXL	<u>230.21</u>	**24.62**	**25.58**	**28.06**	1	27.5GB
	Ours$_{1.4}$	**228.87**	<u>23.74</u>	<u>27.76</u>	26.07	33	8.6GB

results at 512×512 because both our method and *Multi-Diffusion* generate same outputs as the base *Stable Diffusion* model. We also omitted the results of *MultiDiffusion* at 256×256 since it is not designed to generate images at sizes smaller than the base model. Fig. 8 presents generated samples at various aspect ratios. We observe a similar trend of pattern repetition and reduced perceptual quality for images generated by the baselines, in contrast to those generated by ElasticDiffusion. Finally, we apply our method using *SDXL* as the base model to enable Full-HD image generation (1920×1080) and provide examples in Supp. Sec. 9.3.

5.2. Quantitative Results

Table 1 shows quantitative evaluations. *StableDiffusion* shows increasing image quality degradation, as indicated by the *FID* metric when processing images of sizes different from its training resolution 512×512. *MultiDiffusion* slightly improves *FID* at the expense of a substantially more forward calls. *SDXL* demonstrates similar declines in quality at resolutions far from its fine-tuning size of 1024×1024. ElasticDiffusion, however, improves *FID* while maintaining a comparable *CLIP-score* to the base model. ElasticDiffusion also significantly improves the performance for lower resolutions 256×256, while achieving comparable results to *SDXL* at its training resolution 1024×1024, with only $\sim 31\%$ of the memory requirement for *SDXL*.

Table 2. **Quantitative comparison of on LAION-COCO datasets at various aspect ratios (A) and resolutions (R).** best performances are in **bold**, andthe second best are underlined. Vertical means the resolution is transposed from H:W to W:H.

A	R	Method	Horizontal		Vertical	
			FID ↓	CLIP↑	FID ↓	CLIP↑
3:4	384 × 512	SD$_{1.4}$	38.86	24.63	17.66	26.54
		MD$_{1.4}$	–	–	–	–
		SDXL	104.84	21.33	68.84	22.40
		Ours$_{1.4}$	**35.10**	**24.91**	**15.50**	**27.33**
	512 × 680	SD$_{1.4}$	45.54	**24.96**	**16.81**	**27.33**
		MD$_{1.4}$	43.44	24.56	19.13	26.80
		SDXL	62.80	24.20	28.23	26.17
		Ours$_{1.4}$	**41.06**	24.40	18.90	26.83
	768 × 1024	SD$_{1.4}$	71.00	24.09	28.83	26.30
		MD$_{1.4}$	54.89	25.02	26.35	26.95
		SDXL	47.05	**25.79**	**19.50**	**27.41**
		Ours$_{1.4}$	**47.03**	24.91	22.52	25.80
9:16	288 × 512	SD$_{1.4}$	23.50	24.69	24.01	24.89
		MD$_{1.4}$	–	–	–	–
		SDXL	121.83	17.65	112.41	18.54
		Ours$_{1.4}$	**23.23**	**25.26**	**22.86**	**26.30**
	512 × 904	SD$_{1.4}$	29.86	25.34	27.45	26.01
		MD$_{1.4}$	26.35	**25.70**	26.70	25.28
		SDXL	29.60	25.40	27.27	26.08
		Ours$_{1.4}$	**22.85**	25.01	**26.68**	**26.12**

Table 2 provides an evaluation on a variety of aspect ratios and resolutions for both horizontal and vertical image resolutions. *StableDiffusion* obtains worse *FID* score with increasing resolutions, while surprisingly maintaining or improving its *CLIP-score*. We posit that since *CLIP-score* quantifies the agreement between the input prompt and the generated image, *StableDiffusion* benefits from generating repetitive textures and artifacts that align closely with the prompt. For example, a photo of repeated lipsticks might align more with the caption *"lipstick"* despite its poor composition. *MultiDiffusion* generally enhances image quality but does not achieve satisfactory performance. *MultiDiffusion* struggles with objects that span the entire image (*e.g.* Fig. 8). Our method consistently improves *FID* over the baseline on horizontal and most vertical resolutions while preserving fidelity to the input prompts, thereby attaining comparable or superior *CLIP-scores*. Remarkably, even with a larger model size and explicit fine-tuning at a similar resolution of 768×1280, *SDXL* only marginally surpasses our method at the 768×1024 resolution.

Table 3. **Ablation analysis of ElasticDiffusion** on 500 images.

Model Details	FID ↓	CLIP ↑
ElasticDiffusion	133.67	25.82
w/o *Resampling*	150.01	23.82
w/o *RRG*	150.64	24.34
w/o *Imp. overlap*, w/ exp. overlap	141.42	25.82

5.3. Ablation study

Tab. 3 presents results of our method when excluding key components, demonstrating that each element improves performance. Fig. 4 illustrates the effectiveness of our proposed implicit overlap method in resolving boundary discontinuities at a reduced computational cost. Fig. 5 highlights the effectiveness of *Reduced-Resolution Guidance* in removing emerging artifacts. Fig. 6 shows the effectiveness of our iterative resampling technique in enhancing details.

6. Discussion and Conclusion

Experimental results highlight the adaptability and effectiveness of ElasticDiffusion at steering diffusion models to produce an array of resolutions and aspect ratios. ElasticDiffusion requires no fine-tuning, consumes a constant memory footprint, enables both increased and reduced resolutions, and can generate a variety of aspect ratios.

ElasticDiffusion, however, does have several practical limitations. First, inaccuracies in estimating the global and local signals may result in artifacts. Although we attempt to mitigate artifacts with our *Reduced-resolution guidance*, it can still generate blurrier outputs. Second, since the global content guidance is initially estimated at the original training resolution of the underlying diffusion model, our method is less effective in generating images at significantly *extended* sizes beyond the training resolution. In particular, at extreme resolutions beyond 4X, our method produces artifacts and images of a lower perceptual quality. We provide examples of these failure cases in Supp. Sec. 10.4.

The main insight underpinning our method is a novel reinterpretation of *classifier-free guidance* in somewhat disentangling both global and local content. Our comprehensive evaluations demonstrate the feasibility of disentangling these signals, yet the full extent of their separation offers an avenue for further exploration in this direction. We hope that our findings inspire future work in investigating the separation of global and local content guidance signals for image synthesis. This separation holds potential for various applications such as selectively manipulating local and global content or enhancing style transfer. Additionally, the rich semantic representation in the class-direction score has the potential for improving discriminative models.

References

[1] Omri Avrahami, Dani Lischinski, and Ohad Fried. Blended diffusion for text-driven editing of natural images. In *2022 IEEE/CVF Conference on Computer Vision and Pattern Recognition (CVPR)*. IEEE, 2022. 2

[2] Arpit Bansal, Hong-Min Chu, Avi Schwarzschild, Soumyadip Sengupta, Micah Goldblum, Jonas Geiping, and Tom Goldstein. Universal guidance for diffusion models, 2023. 2

[3] Omer Bar-Tal, Lior Yariv, Yaron Lipman, and Tali Dekel. Multidiffusion: Fusing diffusion paths for controlled image generation. In *ICML*, 2023. 2, 3, 4, 6

[4] Angela Castillo, Jonas Kohler, Juan C. Pérez, Juan Pablo Pérez, Albert Pumarola, Bernard Ghanem, Pablo Arbeláez, and Ali Thabet. Adaptive guidance: Training-free acceleration of conditional diffusion models, 2023. 2

[5] Duygu Ceylan, Chun-Hao Paul Huang, and Niloy J. Mitra. Pix2video: Video editing using image diffusion. In *ICCV*, 2023. 2

[6] Hyungjin Chung, Jeongsol Kim, Michael T. Mccann, Marc L. Klasky, and Jong Chul Ye. Diffusion posterior sampling for general noisy inverse problems, 2023. 2

[7] Jiwoo Chung, Sangeek Hyun, and Jae-Pil Heo. Style injection in diffusion: A training-free approach for adapting large-scale diffusion models for style transfer, 2024. 2

[8] Prafulla Dhariwal and Alex Nichol. Diffusion models beat gans on image synthesis. In *NeurIPS*, 2021. 2, 3

[9] Ruoyi Du, Dongliang Chang, Timothy Hospedales, Yi-Zhe Song, and Zhanyu Ma. Demofusion: Democratising high-resolution image generation with no $$$. In *CVPR*, 2024. 2

[10] Alexandros Graikos, Srikar Yellapragada, Minh-Quan Le, Saarthak Kapse, Prateek Prasanna, Joel Saltz, and Dimitris Samaras. Learned representation-guided diffusion models for large-image generation, 2024. 2

[11] Jiatao Gu, Qingzhe Gao, Shuangfei Zhai, Baoquan Chen, Lingjie Liu, and Josh Susskind. Control3diff: Learning controllable 3d diffusion models from single-view images. In *3DV24*, 2023. 2

[12] Lanqing Guo, Yingqing He, Haoxin Chen, Menghan Xia, Xiaodong Cun, Yufei Wang, Siyu Huang, Yong Zhang, Xintao Wang, Qifeng Chen, Ying Shan, and Bihan Wen. Make a cheap scaling: A self-cascade diffusion model for higher-resolution adaptation, 2024. 2

[13] Moayed Haji-Ali, Andrew Bond, Tolga Birdal, Duygu Ceylan, Levent Karacan, Erkut Erdem, and Aykut Erdem. Vidstyleode: Disentangled video editing via stylegan and neuralodes. In *ICCV*, 2023. 13

[14] Feihong He, Gang Li, Lingyu Si, Leilei Yan, Shimeng Hou, Hongwei Dong, and Fanzhang Li. Cartoondiff: Training-free cartoon image generation with diffusion transformer models, 2023. 2

[15] Yingqing He, Shaoshu Yang, Haoxin Chen, Xiaodong Cun, Menghan Xia, Yong Zhang, Xintao Wang, Ran He, Qifeng Chen, and Ying Shan. Scalecrafter: Tuning-free higher-resolution visual generation with diffusion models, 2023. 2

[16] Yingqing He, Tianyu Yang, Yong Zhang, Ying Shan, and Qifeng Chen. Latent video diffusion models for high-fidelity long video generation, 2023. 2

[17] Amir Hertz, Ron Mokady, Jay Tenenbaum, Kfir Aberman, Yael Pritch, and Daniel Cohen-Or. Prompt-to-prompt image editing with cross attention control. In *ICLR*, 2022. 2

[18] Martin Heusel, Hubert Ramsauer, Thomas Unterthiner, Bernhard Nessler, and Sepp Hochreiter. Gans trained by a two time-scale update rule converge to a local nash equilibrium. In *NIPS*, 2017. 6

[19] Jonathan Ho and Tim Salimans. Classifier-free diffusion guidance, 2022. 2

[20] Jonathan Ho, Chitwan Saharia, William Chan, David J. Fleet, Mohammad Norouzi, and Tim Salimans. Cascaded diffusion models for high fidelity image generation. *Journal of Machine Learning Research*, 23(47):1–33, 2022. 2

[21] Jonathan Ho, Tim Salimans, Alexey Gritsenko, William Chan, Mohammad Norouzi, and David J. Fleet. Video diffusion models. In *NeurIPS*, 2022. 2

[22] Edward J. Hu, Yelong Shen, Phillip Wallis, Zeyuan Allen-Zhu, Yuanzhi Li, Shean Wang, Lu Wang, and Weizhu Chen. Lora: Low-rank adaptation of large language models. In *ICLR*, 2022. 2

[23] Rongjie Huang, Jiawei Huang, Dongchao Yang, Yi Ren, Luping Liu, Mingze Li, Zhenhui Ye, Jinglin Liu, Xiang Yin, and Zhou Zhao. Make-an-audio: Text-to-audio generation with prompt-enhanced diffusion models. In *ICML*, 2023. 2

[24] Hugging Face. Stable diffusion xl. https://huggingface.co/docs/diffusers/main/en/using-diffusers/sdxl, 2023. Accessed: [Insert Date Here]. 12

[25] Yujin Jeong, Wonjeong Ryoo, Seunghyun Lee, Dabin Seo, Wonmin Byeon, Sangpil Kim, and Jinkyu Kim. The power of sound (tpos): Audio reactive video generation with stable diffusion. In *ICCV*, 2023. 2

[26] Zhiyu Jin, Xuli Shen, Bin Li, and Xiangyang Xue. Training-free diffusion model adaptation for variable-sized text-to-image synthesis, 2023. 2

[27] Tero Karras, Samuli Laine, Miika Aittala, Janne Hellsten, Jaakko Lehtinen, and Timo Aila. Analyzing and improving the image quality of stylegan. In *CVPR*, 2020. 13

[28] Gwanghyun Kim, Taesung Kwon, and Jong Chul Ye. Diffusionclip: Text-guided diffusion models for robust image manipulation. In *CVPR*, 2022. 2

[29] Zhifeng Kong and Wei Ping. On fast sampling of diffusion probabilistic models. In *ICML*, 2021. 2

[30] Junnan Li, Dongxu Li, Caiming Xiong, and Steven Hoi. Blip: Bootstrapping language-image pre-training for unified vision-language understanding and generation, 2022. 6

[31] Jin Liu, Huaibo Huang, Chao Jin, and Ran He. Portrait diffusion: Training-free face stylization with chain-of-painting, 2023. 2

[32] Andreas Lugmayr, Martin Danelljan, Andres Romero, Fisher Yu, Radu Timofte, and Luc Van Gool. Repaint: Inpainting using denoising diffusion probabilistic models. In *CVPR*, 2022. 5

[33] Sicheng Mo, Fangzhou Mu, Kuan Heng Lin, Yanli Liu, Bochen Guan, Yin Li, and Bolei Zhou. Freecontrol: Training-free spatial control of any text-to-image diffusion model with any condition, 2023. 2

[34] Brian B. Moser, Stanislav Frolov, Federico Raue, Sebastian Palacio, and Andreas Dengel. Dynamic attention-guided diffusion for image super-resolution, 2024. 2

[35] Alex Nichol and Prafulla Dhariwal. Improved denoising diffusion probabilistic models. In *ICML*, 2021. 2

[36] Alex Nichol, Prafulla Dhariwal, Aditya Ramesh, Pranav Shyam, Pamela Mishkin, Bob McGrew, Ilya Sutskever, and Mark Chen. Glide: Towards photorealistic image generation and editing with text-guided diffusion models. In *ICML*, 2022. 2, 6, 12

[37] Suraj Patil, Pedro Cuenca, Nathan Lambert, and Patrick von Platen. Stable diffusion with diffusers. *Hugging Face Blog*, 2022. https://huggingface.co/blog/stable_diffusion. 12

[38] Bo Peng, Xinyuan Chen, Yaohui Wang, Chaochao Lu, and Yu Qiao. Conditionvideo: Training-free condition-guided text-to-video generation, 2023. 2

[39] Dustin Podell, Zion English, Kyle Lacey, Andreas Blattmann, Tim Dockhorn, Jonas Müller, Joe Penna, and Robin Rombach. Sdxl: Improving latent diffusion models for high-resolution image synthesis, 2023. 2, 6, 13

[40] Alec Radford, Jong Wook Kim, Chris Hallacy, Aditya Ramesh, Gabriel Goh, Sandhini Agarwal, Girish Sastry, Amanda Askell, Pamela Mishkin, Jack Clark, Gretchen Krueger, and Ilya Sutskever. Learning transferable visual models from natural language supervision. In *ICML*, 2021. 6

[41] Aditya Ramesh, Prafulla Dhariwal, Alex Nichol, Casey Chu, and Mark Chen. Hierarchical text-conditional image generation with clip latents, 2022. 2

[42] Aditya Ramesh, Prafulla Dhariwal, Alex Nichol, Casey Chu, and Mark Chen. Hierarchical text-conditional image generation with clip latents, 2022. 6

[43] Robin Rombach, Andreas Blattmann, Dominik Lorenz, Patrick Esser, and Björn Ommer. High-resolution image synthesis with latent diffusion models. In *CVPR*, 2022. 1, 2, 3

[44] Nataniel Ruiz, Yuanzhen Li, Varun Jampani, Yael Pritch, Michael Rubinstein, and Kfir Aberman. Dreambooth: Fine tuning text-to-image diffusion models for subject-driven generation. In *CVPR*, 2023. 2

[45] Olga Russakovsky, Jia Deng, Hao Su, Jonathan Krause, Sanjeev Satheesh, Sean Ma, Zhiheng Huang, Andrej Karpathy, Aditya Khosla, Michael Bernstein, Alexander C. Berg, and Li Fei-Fei. Imagenet large scale visual recognition challenge, 2015. 6

[46] Chitwan Saharia, Jonathan Ho, William Chan, Tim Salimans, David J. Fleet, and Mohammad Norouzi. Image super-resolution via iterative refinement, 2021. 2

[47] Chitwan Saharia, William Chan, Saurabh Saxena, Lala Li, Jay Whang, Emily Denton, Seyed Kamyar Seyed Ghasemipour, Burcu Karagol Ayan, S. Sara Mahdavi, Rapha Gontijo Lopes, Tim Salimans, Jonathan Ho, David J Fleet, and Mohammad Norouzi. Photorealistic text-to-image diffusion models with deep language understanding. In *NeurIPS*, 2022. 2, 3, 6, 14

[48] Axel Sauer, Frederic Boesel, Tim Dockhorn, Andreas Blattmann, Patrick Esser, and Robin Rombach. Fast high-resolution image synthesis with latent adversarial diffusion distillation, 2024. 2

[49] Christoph Schuhmann, Romain Beaumont, Richard Vencu, Cade Gordon, Ross Wightman, Mehdi Cherti, Theo Coombes, Aarush Katta, Clayton Mullis, Mitchell Wortsman, Patrick Schramowski, Srivatsa Kundurthy, Katherine Crowson, Ludwig Schmidt, Robert Kaczmarczyk, and Jenia Jitsev. Laion-5b: An open large-scale dataset for training next generation image-text models, 2022. 6

[50] Christoph Schuhmann, Andreas A. Köpf, Richard Vencu, Theo Coombes, and Ross Beaumont. Laion coco: 600m synthetic captions from laion2b-en, 2023. 6

[51] Tamar Rott Shaham, Tali Dekel, and Tomer Michaeli. Singan: Learning a generative model from a single natural image. In *ICCV*, 2019. 13

[52] Fengyuan Shi, Jiaxi Gu, Hang Xu, Songcen Xu, Wei Zhang, and Limin Wang. Bivdiff: A training-free framework for general-purpose video synthesis via bridging image and video diffusion models, 2023. 2

[53] Alex Shonenkov, Misha Konstantinov, Daria Bakshandaeva, Christoph Schuhmann, Ksenia Ivanova, and Nadiia Klokova. DeepFloyd. https://www.deepfloyd.ai/, 2023. Accessed: 2023. 14

[54] Jiaming Song, Chenlin Meng, and Stefano Ermon. Denoising diffusion implicit models. In *ICLR*, 2021. 2, 3

[55] Christian Szegedy, Vincent Vanhoucke, Sergey Ioffe, Jonathon Shlens, and Zbigniew Wojna. Rethinking the inception architecture for computer vision. In *CVPR*, 2015. 6

[56] Andrey Voynov, Amir Hertz, Moab Arar, Shlomi Fruchter, and Daniel Cohen-Or. Anylens: A generative diffusion model with any rendering lens, 2023. 2

[57] Bingyuan Wang, Hengyu Meng, Zeyu Cai, Lanjiong Li, Yue Ma, Qifeng Chen, and Zeyu Wang. Magicscroll: Nontypical aspect-ratio image generation for visual storytelling via multi-layered semantic-aware denoising, 2023. 2

[58] Fu-Yun Wang, Zhaoyang Huang, Xiaoyu Shi, Weikang Bian, Guanglu Song, Yu Liu, and Hongsheng Li. Animatelcm: Accelerating the animation of personalized diffusion models and adapters with decoupled consistency learning, 2024. 2

[59] Jianyi Wang, Zongsheng Yue, Shangchen Zhou, Kelvin C. K. Chan, and Chen Change Loy. Exploiting diffusion prior for real-world image super-resolution, 2023. 2, 3, 4

[60] Lezhong Wang, Jeppe Revall Frisvad, Mark Bo Jensen, and Siavash Arjomand Bigdeli. Stereodiffusion: Training-free stereo image generation using latent diffusion models, 2024. 2

[61] Daniel Watson, William Chan, Ricardo Martin-Brualla, Jonathan Ho, Andrea Tagliasacchi, and Mohammad Norouzi. Novel view synthesis with diffusion models. In *ICLR*, 2023. 2

[62] Weihao Xia, Yujiu Yang, Jing-Hao Xue, and Baoyuan Wu. Tedigan: Text-guided diverse face image generation and manipulation, 2021. 6

[63] Guy Yariv, Itai Gat, Lior Wolf, Yossi Adi, and Idan Schwartz. Audiotoken: Adaptation of text-conditioned diffusion models for audio-to-image generation, 2023. 2

[64] Ahmet Burak Yildirim, Vedat Baday, Erkut Erdem, Aykut Erdem, and Aysegul Dundar. Inst-inpaint: Instructing to remove objects with diffusion models, 2023. 2

[65] Jiwen Yu, Yinhuai Wang, Chen Zhao, Bernard Ghanem, and Jian Zhang. Freedom: Training-free energy-guided conditional diffusion model, 2023. 2

[66] Shen Zhang, Zhaowei Chen, Zhenyu Zhao, Zhenyuan Chen, Yao Tang, Yuhao Chen, Wengang Cao, and Jiajun Liang. Hidiffusion: Unlocking high-resolution creativity and efficiency in low-resolution trained diffusion models, 2023. 2

[67] Peiang Zhao, Han Li, Ruiyang Jin, and S. Kevin Zhou. Loco: Locally constrained training-free layout-to-image synthesis, 2024. 2

[68] Qingping Zheng, Yuanfan Guo, Jiankang Deng, Jianhua Han, Ying Li, Songcen Xu, and Hang Xu. Any-size-diffusion: Toward efficient text-driven synthesis for any-size hd images, 2023. 2, 13

[69] Álvaro Barbero Jiménez. Mixture of diffusers for scene composition and high resolution image generation, 2023. 2, 3, 4

Appendices

In this supplementary document, we extended the discussion on existing diffusion models generation processes, highlighting their constraints in adapting to diverse image sizes and the potential for separating global and local content generation. We also provide further qualitative comparisons with baselines using the DrawBench benchmark [36] at various resolutions including full-HD. Our code can be accessed at https://github.com/MoayedHajiAli/ElasticDiffusion-official.git

7. ElasticDiffusion Symbols and Implementation.

To simplify the notation in this paper, we have employed specific symbols to denote the key elements within our framework. To clarify the associations between each symbol and their meanings, we provide in Tab. 4, a detailed explanation of each symbol that we used in the paper. Additionally, we describe in Algorithm 1 the full generation process of an image or arbitrary size $\bar{H} \times \bar{W}$ using a pre-trained base diffusion models that operates on images of size $H \times W$

Table 4. Table of symbols used in this paper.

Symbol	Correspondence
$H \times W$	training resolution of the base diffusion model
$\bar{H} \times \bar{W}$	target resolution of the generated image
$N \times M$	chosen resolution of the same aspect ratio as $\bar{H} \times \bar{W}$ but smaller than $H \times W$
ϵ_θ	pre-trained diffusion model network
w	classifier-free guidance weight
x_t	diffusion latent at timestep t of size $H \times W$
$\bar{x}_t$	diffusion latent at timestep t of size $\bar{H} \times \bar{W}$
$\mathbf{x}_t$	downsampled latent from $\bar{x}_t$
$\hat{\mathbf{x}}_t$	padded $\mathbf{x}_t$ to match the training resolution $H \times W$
$\hat{x}_0^t$	a noise-free sample of x
$\hat{\mathbf{x}}_0^t$	a noise-free sample of $\mathbf{x}$
p_k	a crop of $\bar{x}_t$ smaller than the training resolution
c_k	a context crop of $\bar{x}_t$
$\mathbf{S}_u$	unconditional score for latent at size $H \times W$
$\mathbf{S}_c$	conditional score for latent at size $H \times W$
$\mathbf{S}_d$	class-direction score for latent at size $H \times W$
$\bar{\mathbf{S}}_u$	unconditional score for latent at size $\bar{H} \times \bar{W}$
$\bar{\mathbf{S}}_d$	class-direction score for latent at size $\bar{H} \times \bar{W}$

8. Discussion on Diffusion Models

In this section, we discuss the generation process of diffusion models, focusing on their performance across various image sizes and our analysis of their capacity to separate global and local content generation.

8.1. Diffusion Models Adaptability Across Sizes

Pretrained diffusion models such as *StableDiffusion*$_{1.4}$ are technically capable of handling various image sizes. Accordingly, the official implementation provides parameters for adjusting the size of the generated images. However, our experiments show a significant decline in image quality when these models operate at resolutions outside those seen during training. These observations are confirmed in the Stable Diffusion blog post on Hugging Face which warns that deviating from the trained resolution may compromise image quality [37]. Specifically, it notes that going below the training resolution results in lower quality images, while exceeding it in both the height and width directions causes repetitive image areas, leading to a loss of global coherence. Similar findings were noted in the *StableDiffusion-XL* official blog post [24].

In Fig. 9, we qualitatively analyze how generating images larger than the training resolution impacts image coherence. We generate these results using *StableDiffusion*$_{1.4}$ which was pretrained on 512×512 images. For smaller dimensions, the model tends to stretch the generated objects, whereas for larger dimensions, such as 1024×1024, it often creates repetitive

Algorithm 1 Sampling Algorithm for Image at $\bar{H} \times \bar{W}$

Require:

    ϵ_θ $\triangleright$ pre-trained DM at $H \times W$

    c, w $\triangleright$ text condition and CFG weight

    $\bar{x}_T \sim \mathcal{N}(0, I)$ $\triangleright$ noise at $\bar{H} \times \bar{W}$

1: **for** $t = T$ **down to** 1 **do**
2:     $\mathbf{x}_t \leftarrow \text{Downsample}(\bar{x}_t, N \times M)$
3:     $\mathcal{Z}_t \sim \mathcal{N}(0, I)$
4:     $\mathcal{A}_t \leftarrow \mathcal{Y}_{H-N, W-M}, \mathcal{Y} \sim \text{Uniform}(0, 255)$
5:     $\hat{\mathbf{x}}_t \leftarrow \text{Pad}\left(\mathbf{x}_t, \mathcal{A}_t \sqrt{\bar{\alpha}_t} + \sqrt{1 - \bar{\alpha}_t} \cdot \mathcal{Z}_t\right)$ $\triangleright$ Pad to match training resolution $H \times W$
6:     $\mathbf{S}_c \leftarrow \text{Crop}\left(\epsilon_\theta\left(\hat{\mathbf{x}}_t, c\right), N \times M\right)$ $\triangleright$ conditional score at target aspect ratio
7:     $\mathbf{S}_u \leftarrow \tilde{\epsilon}_\theta(\hat{\mathbf{x}}_t)$ $\triangleright$ Uncodnitional score from Eq. (3)
8:     $\bar{\mathbf{S}}_d^0 \leftarrow \text{Upsample}(\mathbf{S_c} - \hat{\mathbf{S}}_\mathbf{u}, \bar{H} \times \bar{W})$ $\triangleright$ class-direction score
9:     **for all** $r = 1, \ldots, R$ **do**
10:         $\bar{\mathbf{S}}_d^r \leftarrow \text{Resample}(\bar{\mathbf{S}}_d^{r-1}, \bar{x}_t)$ $\triangleright$ Eq. (6)
11:     **end for**
12:     $\bar{\mathbf{S}}_\mathbf{u} \Leftarrow \tilde{\epsilon}_\theta(\bar{x}_t)$ $\triangleright$ Eq. (3)
13:     $\bar{x}_{t-1} \leftarrow \bar{\mathbf{S}}_u + (1 + w) \cdot \bar{\mathbf{S}}_d^R$ $\triangleright$ diffusion update
14:     $\bar{x}_{t-1} \leftarrow \bar{x}_{t-1} - \text{RRG}(\bar{x}_t, \mathbf{x}_t)$ $\triangleright$ Eq. (7)
15: **end for**
16: **return** $\bar{x}_0$

---

elements. Notice the stretch in the cat and lion faces in the third and fourth columns. Additionally, observe how artifacts and repetition regarding nose and eye parts tend to happen more frequently as we increase the resolution.

Notably, the model maintains its output quality within a narrow margin of 64 pixels from its training resolution, suggesting a limit to the generalization capabilities of diffusion models with respect to various image sizes. This observation also shows the potential limitations of the solutions based only on a fine-tuning process for a fixed set of aspect ratios such as those proposed in prior work [39, 68].

8.2. Global and Local Content Generation

In the domain of generative adversarial networks (GANs), the disentanglement style and content in the synthesized images has been widely explored, paving the way for advancements in diverse generation and editing applications [13, 27, 51]. However, the precise definitions of 'style' and 'content' remain fluid, with no consensus on the definition in the literature. Previous works often define the content and style based on manually pre-defined attributes. In this work, we opt to avoid such ambiguity by denoting the overall composition of the image as global content and the fine-grained details as local content. Subsequently, we conceive ElasticDiffusion based on two key insights: First, the *class direction score* (Eq. (2) in the main paper) collectively influences pixels to shape the overall composition of the generated image, denoted as global content. This global score can be effectively shared among neighboring pixels. Fig. 10 demonstrates that sharing the *class direction score* between nearby pixels maintains the global content and coherence of the generated image, although increasing the sharing extent decreases the perceptual quality. In contrast, the *unconditional score* requires pixel-level precision and it may not be feasible to share it between nearby pixels, as illustrated in Fig. 11. Second, the *unconditional score* dictates the fine-grained details of the generated image, denoted as local content. This suggests that the score can be computed effectively on localized regions without necessitating global information from the entire image. Fig. 12 shows that computing the *unconditional score* in localized regions, corresponding to the size 512×512 of the generated image, produces similar results to those obtained when computing the score globally.

9. Analysis of ElasticDiffusion

This section provides a comprehensive analysis of ElasticDiffusion, focusing on its application to pixel-based diffusion models and comparisons with baseline methods. We present further qualitative results to showcase ElasticDiffusion's effectiveness in enhancing the coherence of the generated image across various sizes. We finally discuss the limitations and failure cases of our method.

9.1. Additional Ablation Study.

To better understand the effect of the class-direction refinement and reduced-resolution guidance (RRG) strategy on the overall quality of the results, we analysed in Tab. 5 the performance of ElasticDiffusion when excluding these components at two different resolutions. We observe that their necessity is pronounced at higher resolutions (e.g., 4x), while their influence is limited at lower upsampling scale (e.g., 2x). Notably, even without these components, our method achieves *better* FID than baselines.

	768×768		1024×1024	
	FID $\downarrow$	CLIP $\uparrow$	FID $\downarrow$	CLIP $\uparrow$
Ours	225.86	26.66	228.87	23.74
w/o RRG	230.27	24.13	234.66	23.15
w/o RGG & refined class-direction score	233.49	23.32	263.15	20.91

Table 5. **Ablation study** on CelebAHQ Dataset using *StableDiffison*$_{1.4}$ as the base model.

9.2. Generalization to Pixel-Based Diffusion Models

We apply ElasticDiffusion to a pre-trained *DeepFloyd-IF-XL-V1.0* model, which operates on the pixel-space [53]. In the first stage, *DeepFloyd-XL-V1.0* generates images at a 64×64 resolution, which are then upscaled to 256×256 and subsequently to 1024×1024 in later stages. To assess the generalization capabilities of our method, we only focus on the first stage which generates images at a low resolution. As illustrated in Fig. 13, *DeepFloyd-XL-V1.0* shows similar limitations as latent diffusion models when dealing with various resolutions, primarily characterized by repetitive elements and reduced image coherence. However, we demonstrate the effectiveness of ElasticDiffusion in enhancing the ability of the pre-trained model to handle diverse resolutions and aspect ratios by successfully generating well-structured images. This shows the applicability of our proposed generation process to diffusion models that operate on the pixel space.

9.3. Additional Qualitative Results

We provide further qualitative analysis of ElasticDiffusion.

Figure 14 provides a comparison with *StableDiffusion* and *MultiDiffusion* using selected DrawBench [47] prompts for horizontal images at resolution 680×512. We highlight the tendency of baseline methods to generate repetitive elements. This not only disrupts the image's overall coherence but also makes the baselines struggle to accurately reflect object counts. For example, in the first row, both baselines produced multiple dogs for an input prompt '*one* dog on the street'. In contrast, our method effectively aligns with the given prompt, generating a single, coherent dog.

Figure 15 shows a similar analysis on vertical images of resolution 512×680. We observe a similar limitation in baselines such as element and texture repetition in the generated images. This tendency of repeating elements particularly affects the model's capacity to create coherent objects that share textures with the background. For example, In the first row, the baselines struggle to accurately depict a hamburger, whereas our method successfully generates a coherent hamburger that is separated from the background. This limitation also affects the baseline models' ability to render objects with repeating patterns, like a 'cube made of bricks' shown in the last row. Moreover, the baseline behavior of repeating patterns especially escalates when generating a single object across the majority of the image, as observed in the 4th and 5th rows. In contrast, our method is able to maintain image coherence across various settings.

Figures 16 and 17 focus on showing results for the generation of Full-HD horizontal images using *StableDiffusion-XL* as the base model. We compare against the standard decoding process of *StableDiffusion-XL* on sampled DrawBench prompts from the Reddit Category and observe a significant improvement in image coherence when applying our method. Notice in Fig. 16 how *StableDiffusion-XL* stretch the car in the first example, or repeat the limbs of the corgi and the lion (in the 2nd and 3rd example). In comparison, our method successfully coherently generates the requested image without any such distortions, all while utilizing lower memory requirements.

Figures 18 and 19 provide a similar analysis for Full-HD vertical images. *StableDiffusion-XL* produces significantly distorted images which either contain incorrectly repeating elements as seen in the cat and the man faces in the first two examples of Fig. 18, or stretched parts like the woman face in the first example of Fig. 19. In contrast, our method generates detailed objects that fit the vertical aspect ratio while avoiding any stretching or element repetition.
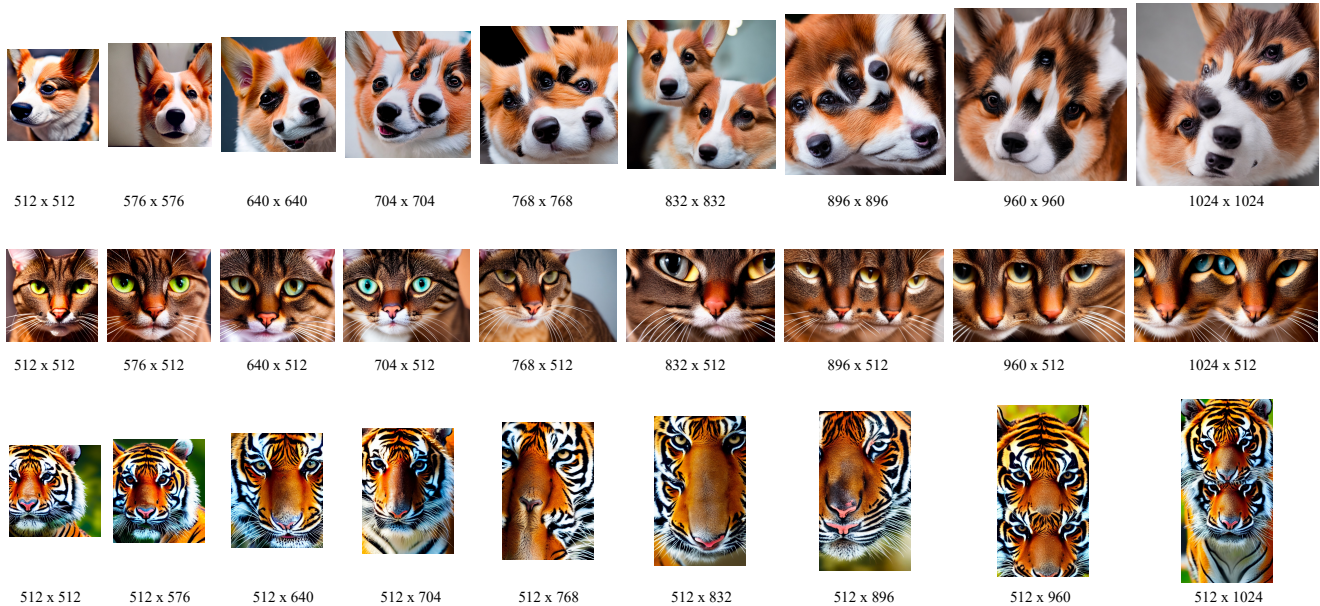
Figure 9. **Degradation of image quality in StableDiffusion₁.₄ with varying resolutions.** We illustrate the progressive decrease in image quality as the resolution deviates from the model's training size of 512×512. The results on square, horizontal, and vertical resolutions show a significant reduction in global coherence for image sizes beyond 64 pixels from the training resolution.

9.4. Limitations

Fig. 20 illustrates the limitations of ElasticDiffusion in various scenarios. Our method retains some limitations of the pre-trained base model, including challenges with text-image alignment for complex prompts and occasional occurrence of artifacts. Additionally, we observe an increase in image blurriness with the application of larger *Reduced-Resolution Guidance* weights (Sec. 4.4 of the main paper). Moreover, while infrequent, there are instances where the constant-color background inadvertently blends into the generated image (as discussed in Sec. 4.2 of the main paper).
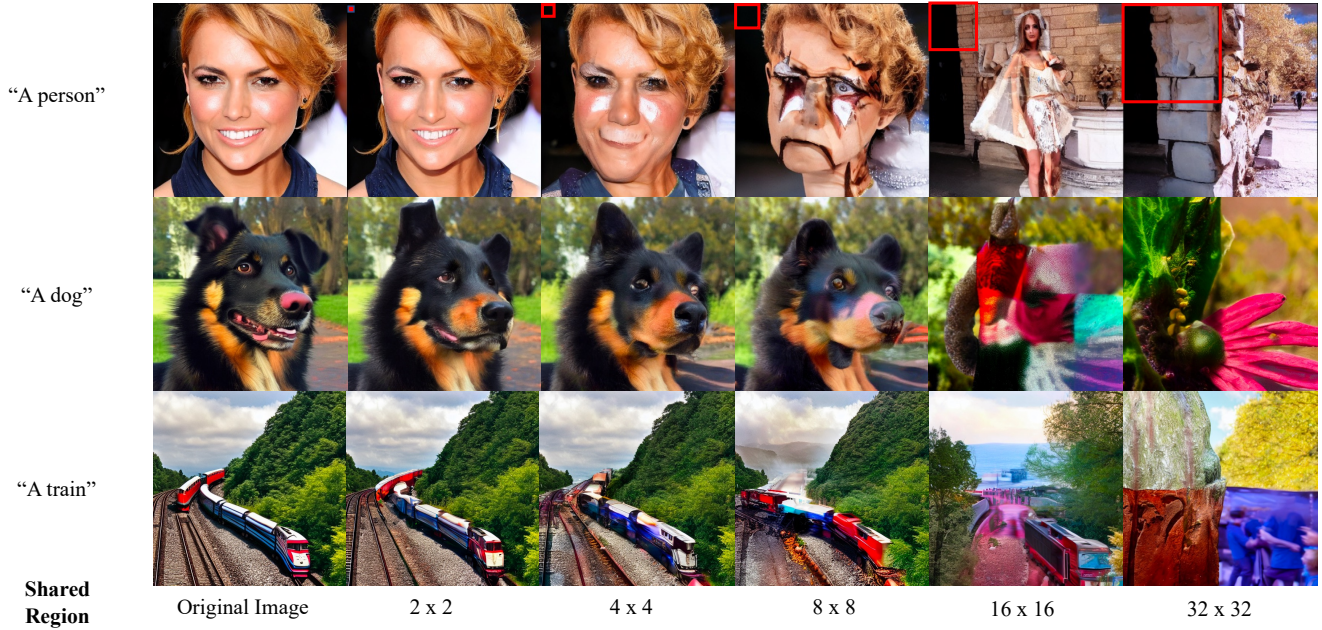
Figure 10. **Effect of sharing *class direction score* between nearby pixels.** We highlight that sharing the score within a group of neighboring pixels preserves the global content and coherence of the image, despite a reduction in the perceptual quality when selecting larger group sizes (as denoted by the red square). This supports our assumption that this score tends to be similar among neighboring pixels. To conduct this experiment, we downsample the *class direction score* of size 64×64 by a factor $N \times M$ (as specified in the last row) and upsample it back to 64×64, thus sharing the score for each $N \times M$ region. Note that as our experiments utilize a latent diffusion model, sharing the score within an $N \times M$ latent pixels during the decoding process impacts $8N \times 8M$ pixels of the final generated image.
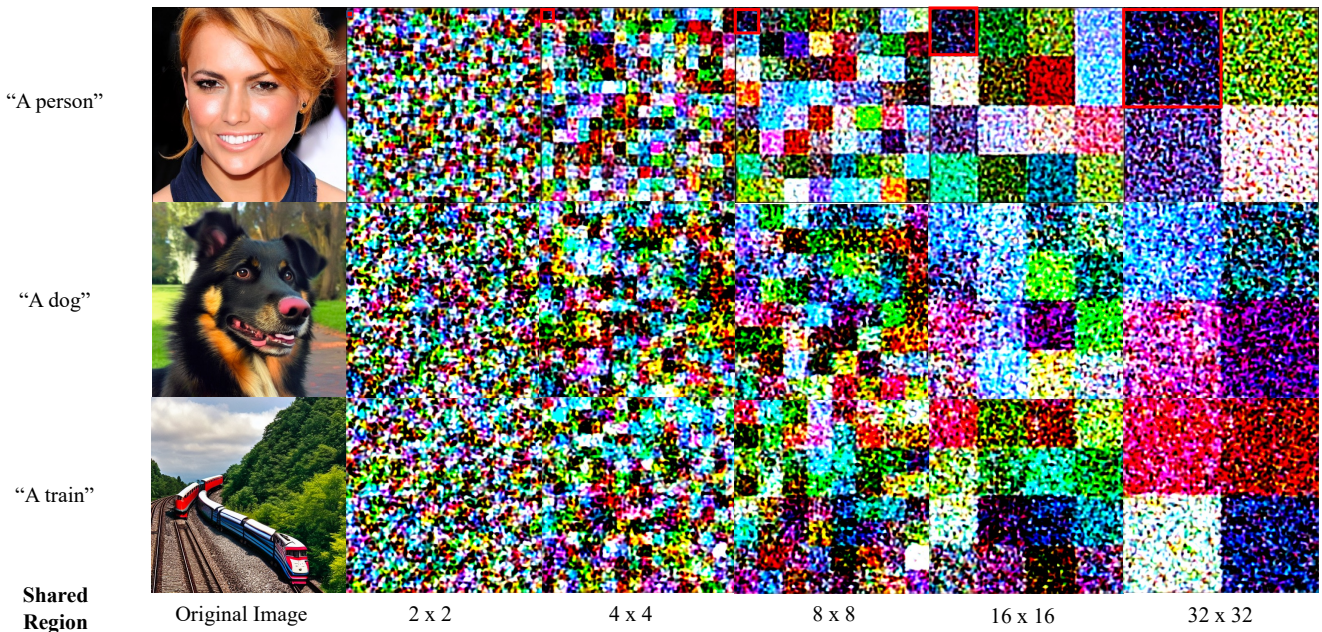
Figure 11. **Effect of sharing *unconditional score* between nearby pixels.** We show that sharing the unconditional score, even in small groups of pixels, leads to the generation of complete noise. This indicates that *uncondtional score*, in contrast to the *class direction score*, requires pixel-level precision to generate local details.
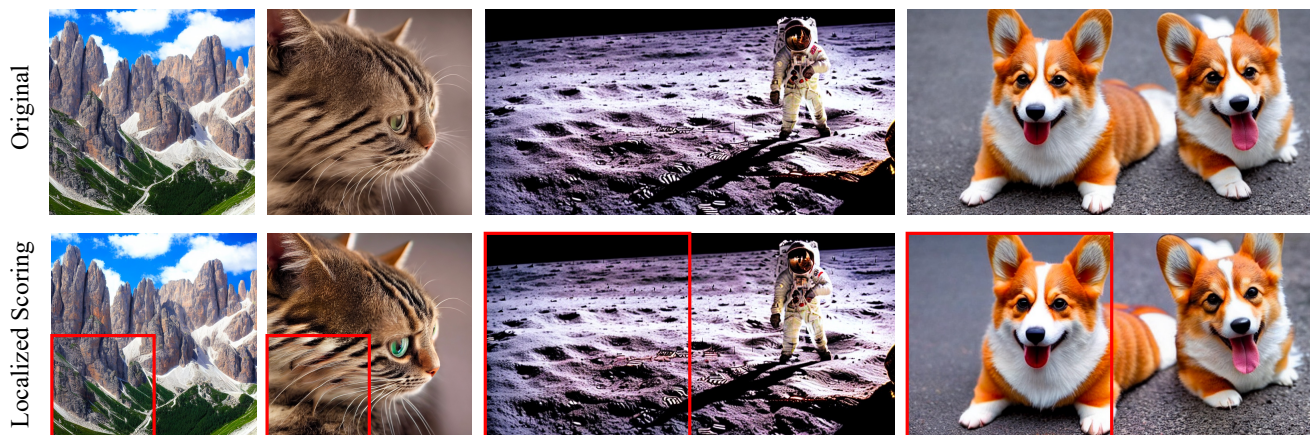
Figure 12. **Unconditional score computation on localized regions.** We show that computing the diffusion model *unconditional score* on local patches (corresponding to the size of the red boxes in the second row) results in images that are visually similar to those produced by a global score computation (displayed in the first row).

96 x 96: A teddy bear   *128 x 128:* A cat   *128 x 64:* A person   *64 x 128:* A person

Ours   *DeepFloyd-XL*   **Ours**   *DeepFloyd-XL*   **Ours**   *DeepFloyd-XL*   **Ours**   *DeepFloyd-XL*

Figure 13. ***DeepFloyd-XL* across various image sizes.** We test *DeepFloyd-XL*, a diffusion model that operates on the pixel space, across multiple image resolutions. We observe a degradation in performance similar to that seen in $StableDiffusion$. The application of ElasticDiffusion significantly improves the overall composition of the generated images.

One dog on the street.
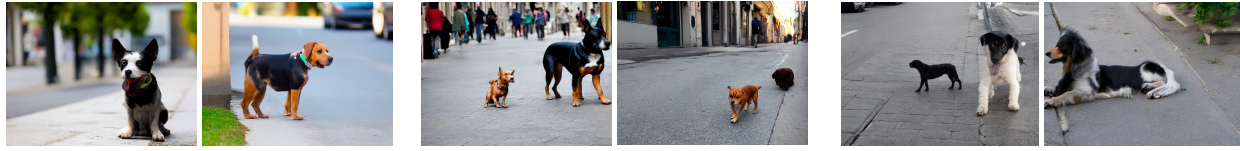
A fisheye lens view of a turtle sitting in a forest.

One cat and one dog sitting on the grass.

Illustration of a mouse using a mushroom as an umbrella.

In late afternoon in January in New England, a man stands in the shadow
of a maple tree.

A large keyboard musical instrument with a wooden case enclosing a soundboard and
metal strings, which are struck by hammers when the keys are depressed.

| *Ours* | *StableDiffusion* | *MultiDiffusion* |

Figure 14. **Additional qualitative comparison on horizontal images using selected DrawBench prompts.** We use $SD_{1.4}$ as a base model for our method, *StableDiffusion*, and *MultiDiffusion* and generate images at resolution 680×512. Images produced by baselines display reduced alignment to the input prompt (1st and 3rd rows) and repeated elements (4th and 6th rows). In comparison, our method displays superior image coherence and faithfulness to the input prompts.

Figure 15. **Additional qualitative comparison on vertical images using selected DrawBench prompts.** We use $SD_{1.4}$ base model for our method, *StableDiffusion*, and *MultiDiffusion* and generate at the resolution 512×680. Similar to the horizontal resolutions, baseline methods exhibit several limitations such as poor text-image alignment (1st and 2nd rows), repeated elements (3rd, 4th and 5th rows), and generated artifacts (6th and 7th rows). In comparison, our method consistently maintains better image coherence and fidelity to the input prompts.

A car playing soccer, digital art.

A realistic photo of a Pomeranian dressed up like a 1980s professional wrestler with neon green and neon orange face paint and bright green wrestling tights with bright orange boots.

A tiger in a lab coat with a 1980s Miami vibe, turning a well oiled science content machine, digital art.
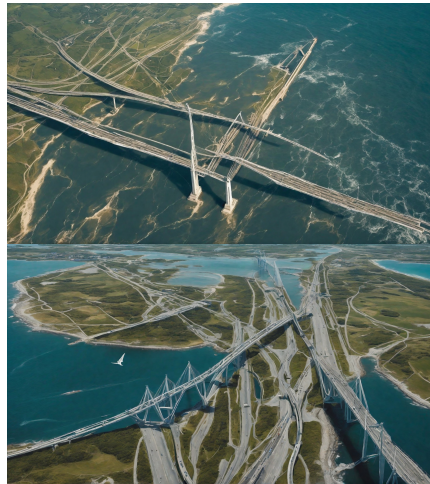
Ours   *StableDiffusion-XL*

Figure 16. **Additional qualitative comparison with SDXL on Full-HD horizontal images**. We use randomly sampled DrawBench prompts from the Reddit Category. Despite its fine-tuning process, *StabelDiffusion-XL* produces images with repetitive textures and elements in full-HD resolution. Our method achieves a more cohesive composition while maintaining a comparable level of details, all while requiring less memory.
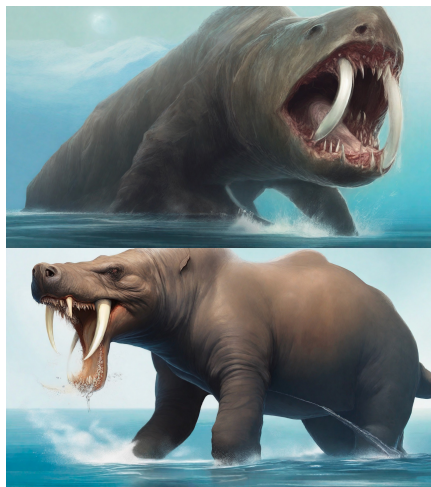
A fluffy baby sloth with a knitted hat trying to figure out a laptop, close up, highly detailed, studio lighting, screen reflecting in its eyes.

A bridge connecting Europe and North America on the Atlantic Ocean, bird's eye view.

A large thick-skinned semiaquatic African mammal, with massive jaws and large tusks.

Ours   *StableDiffusion-**XL***

Figure 17. **Additional qualitative comparison with SDXL on Full-HD horizontal images**. We use randomly sampled DrawBench prompts from the Reddit Category. *StabelDiffusion-XL* produce images that tend to repeat body parts and texture in full-HD resolution. In comparison, our method achieves better image coherence and maintains a similar perceptual quality, all while requiring less memory.

Photo of an athlete cat explaining it's latest scandal at a press conference to journalists.

An oil painting portrait of the regal Burger King posing with a Whopper.

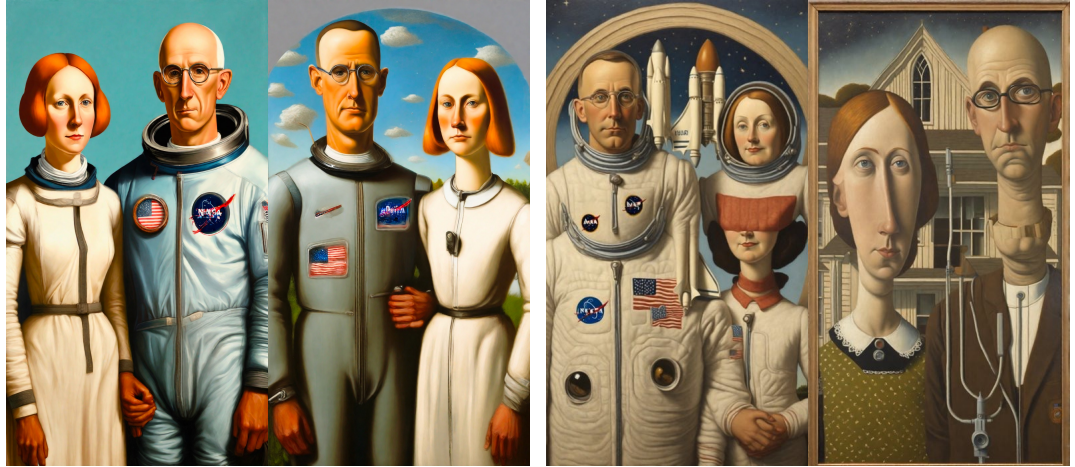*A 1960s yearbook photo with animals dressed as humans.*

Ours **StableDiffusion-XL**

Figure 18. **Additional qualitative comparison with SDXL on Full-HD vertical images**. We use randomly sampled DrawBench prompts from the Reddit Category. Similar to horizontal resolutions, *StabelDiffusion-XL* produce repeated elements in full-HD resolution. In comparison, our method achieves more coherent images and generates content that fits the frame aspect ratio.

A painting by Grant Wood of an astronaut couple, american gothic style.

Colouring page of large cats climbing the eifel tower in a cyberpunk future.

An old photograph of a 1920s airship shaped like a pig, floating over a wheat field.

Ours *StableDiffusion-XL*

Figure 19. **Additional qualitative comparison with SDXL on Full-HD vertical images**. We use randomly sampled DrawBench prompts from the Reddit Category. Similar to horizontal resolutions, *StabelDiffusion-XL* produce repeated elements that significantly affect the image coherence. In comparison, our method achieves superior composition while maintaining a similar level of detail.

A pear cut into **seven pieces**.
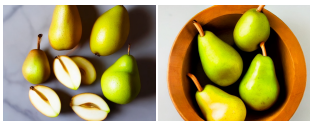
(A) Poor Image-text alignment   (C) Blurry Outputs   (B) Emerging Artifacts   (D) Background Bleedthrough

Figure 20. **Limitations of ElasticDiffusion.** (A) poor text-image alignment for complex prompts, inherited from the base diffusion model, (B) increased blur in outputs with higher RRG weight, (C) emerging artifacts in complex images, and (D) rare background bleed-through where the color-constant background is unintentionally included in the generated image.